Electric-field-induced displacement of a charged spherical colloid embedded in an elastic Brinkman medium

Reghan J. Hill*
Department of Chemical Engineering and McGill Institute for Advanced Materials, McGill University, Montreal, Quebec, Canada H3A 2B2

M. Ostoja-Starzewski
Department of Mechanical Science and Engineering, University of Illinois at Urbana-Champaign, Urbana, Ilinois 61801, USA
(Received 5 October 2007; published 25 January 2008)

When an electric field is applied to an electrolyte-saturated polymer gel embedded with charged colloidal particles, the force that must be exerted by the hydrogel on each particle reflects a delicate balance of electrical, hydrodynamic, and elastic stresses. This paper examines the displacement of a single charged spherical inclusion embedded in an uncharged hydrogel. We present numerically exact solutions of coupled electrokinetic transport and elastic-deformation equations, where the gel is treated as an incompressible, elastic Brinkman medium. This model problem demonstrates how the displacement depends on the particle size and charge, the electrolyte ionic strength, and Young's modulus of the polymer skeleton. The numerics are verified, in part, with an analytical (boundary-layer) theory valid when the Debye length is much smaller than the particle radius. Finally, we identify a close connection between the displacement when a colloid is immobilized in a gel and its velocity (electrophoretic mobility) when dispersed in a Newtonian electrolyte.

DOI: 10.1103/PhysRevE.77.011404 PACS number(s): 82.70.Dd

I. INTRODUCTION

Hydrogels are soft, water-saturated networks of polymer with molecular-scale porosity. They find widespread use in molecular-separation technologies (gel electrophoresis), drug delivery, scaffolds for tissue engineering, cell culture, wound care (e.g., [1,2]), and microfluidic pumping and control (e.g., [3]).

This paper concerns a class of hydrogel composites where charged colloidal inclusions are immobilized in an uncharged hydrogel matrix. Matos *et al.* [4] recently demonstrated that polyacrylamide hydrogels doped with silica nanoparticles significantly enhance the electric-field-induced transport of both charged and uncharged molecules through the composite. Each charged inclusion experiences electrical, hydrodynamic, and mechanical contact forces, while the mobile countercharge produces an electro-osmotic flow that permeates the surrounding polymer. Note that electrokinetic theory quantifies how the charge and size of the inclusions, the ionic strength of the electrolyte, and permeability of the gel influence the electro-osmotic pumping capacity of the composite [5], but little is known of the particle displacement and flow-induced distortion of the polymer matrix.

The particle displacement could be used as a diagnostic to probe the physicochemical characteristics of the particle-polymer interface, much like the electric-field-induced particle velocity (electrophoretic mobility) is used to infer the so-called ζ potential of colloidal particles dispersed in Newtonian electrolytes. Also, knowledge of the microscale strain field in the hydrogel is essential for establishing the electric field strength required to initiate microscale fracture. Finally, the relationship between particle displacement and the elastic and viscous characteristics of the surrounding matrix is central to the rapidly advancing field of microrheology [6,7], which seeks to quantify the dynamics and structure of complex fluids [8,9].

In this work, our principal objective is to quantify how the particle, electrolyte and hydrogel characteristics influence the electric-field-induced particle displacement. As a first step, we solve a model problem where classical electrokinetic transport processes are coupled to the deformation of an incompressible isotropic, homogeneous porous medium. The analysis is restricted to situations where the applied electric field is uniform and weak, so the particle displacement is small and perturbations to equilibrium may be linearized accordingly. In this manner, our approximations are similar to those widely adopted in the classical theories of microelectrophoresis [10] and other phoretic motion [11]. Nevertheless, our calculations are not restricted by the magnitude of the particle ζ potential or the thickness of the equilibrium diffuse layer of counterions (Debye length).

Before presenting the full model and examining the results, it is instructive to first consider the expected displacement Z of an inclusion if the bare electrical force $\sigma 4\pi a^2 E$ is balanced by an elastic restoring force $2\pi a\mathcal{E}Z$. Here, σ is the surface charge density, $4\pi a^2$ is the surface area, E is the electric-field strength, and $\mathcal{E}$ is Young's modulus of the gel. Accordingly, the particle displacement is [12]

$$Z = 2\sigma a\mathcal{E}^{-1}E. \tag{1}$$

Equation (1) overestimates the displacement by a factor of $(2/3)\kappa a$ when $\kappa a \to \infty$ and $|\zeta| < kT/e$. Note that κa is the particle radius a scaled with the Debye length κ^{-1}, ζ is the ζ potential, kT is the thermal energy, and e is the fundamental

*Author to whom correspondence should be addressed; reghan.hill@mcgill.ca

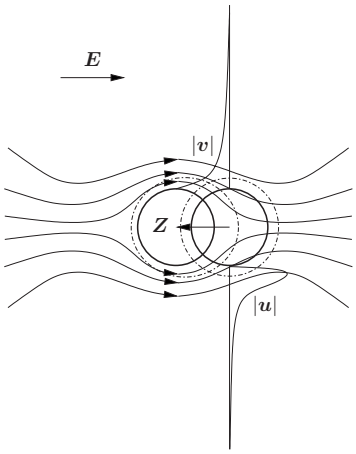

FIG. 1. Schematic representation of a (negatively) charged, spherical colloid embedded in an unbounded electrolyte-saturated, elastic polymer gel (elastic Brinkman medium). An electric field $\boldsymbol{E}$ is applied that drives electro-osmotic flow $\boldsymbol{u}$, which, in turn, exerts a body force on the gel that induces a displacement field $\boldsymbol{v}$. The net result of the electrical, hydrodynamic, and elastic stress is a displacement $\boldsymbol{Z}$ of the particle (to the left-hand side). The dashed lines denote the equilibrium (right-hand side) and polarized (left-hand side) diffuse double layers. In the far field ($r\to\infty$), the velocity and displacement fields decay as r^{-3}. In this work, the displacement field is treated as the sum of two fields that each decay as r^{-1}; one is induced by a particle displacement $\boldsymbol{Z}\neq\boldsymbol{0}$ with $\boldsymbol{E}=\boldsymbol{0}$, and the other is the flow-induced distortion with $\boldsymbol{E}\neq\boldsymbol{0}$ and $\boldsymbol{Z}=\boldsymbol{0}$.

charge. When $\kappa a\to 0$ and $|\zeta|<kT/e$, however, Eq. (1) becomes

$$Z=2\zeta\epsilon_s\epsilon_o\mathcal{E}^{-1}E \quad (\kappa a\to 0,|\zeta|<kT/e). \tag{2}$$

Equation (2) and the correct form of Eq. (1) for $\kappa a\to\infty$ (see Sec. V) are, respectively, reminiscent of the well-known Hückel and Smoluchowski limits for the electrophoretic mobility [10]. Indeed, despite obvious differences, the inclusion displacement and electrophoretic velocity have a remarkably similar and, in general, complicated dependence on the scaled particle size κa and scaled ζ potential $\zeta e/(kT)$.

II. MODELS FOR ELECTROKINETIC TRANSPORT AND ELASTIC DEFORMATION

As depicted in Fig. 1, we consider a single spherical colloid with radius a and surface charge density σ embedded in an unbounded, electrically neutral hydrogel. The gel is modeled as a homogeneous Brinkman medium [13] that is saturated with an aqueous electrolyte (e.g., NaCl). Together, the electrolyte concentration, surface charge density and particle radius manifest as an electrostatic potential ζ at the colloid surface ($r=a$). Note that the countercharge is concentrated in a diffuse layer with thickness (Debye length) κ^{-1}.

A. Electrokinetic transport

The electrokinetic model used in this work to calculate the equilibrium and perturbed electrolyte ion concentrations, pressure, and fluid velocity is a straightforward extension of the *standard electrokinetic model* [14] widely used to describe microelectrophoresis and other electrokinetic phenomena. Details have been presented elsewhere [5,15]. The full set of (steady) transport equations is

$$\epsilon_o\epsilon_s\nabla^2\psi=-\sum_{j=1}^{N}n_jz_je, \tag{3}$$

$$\boldsymbol{j}_j=n_j\boldsymbol{u}-z_jen_j\frac{D_j}{kT}\boldsymbol{\nabla}\psi-D_j\boldsymbol{\nabla}n_j, \tag{4}$$

$$\eta\nabla^2\boldsymbol{u}-\boldsymbol{\nabla}p=(\eta/\ell^2)\boldsymbol{u}+\sum_{j=1}^{N}n_jz_je\boldsymbol{\nabla}\psi, \tag{5}$$

with (steady) ion and electrolyte conservation equations

$$\boldsymbol{\nabla}\cdot\boldsymbol{j}_j=0 \quad \text{and} \quad \boldsymbol{\nabla}\cdot\boldsymbol{u}=0.$$

The electrostatic potential, N ion concentrations and fluxes, electrolyte velocity, and pressure are denoted ψ, n_j and $\boldsymbol{j}_j$, $\boldsymbol{u}$, and p, respectively. Other variables are the solvent dielectric constant ϵ_s, permittivity of a vacuum ϵ_o, fundamental charge e, ion valances z_j and diffusion coefficients D_j, thermal energy kT, solvent viscosity η, and Darcy permeability ℓ^2. The Brinkman screening length ℓ denotes the characteristic length scale over which the fluid velocity disturbance produced by a net force decays in the porous medium [13]. Equivalently, the product $(\eta/\ell^2)\boldsymbol{u}$ is readily interpreted as a body force (often termed Darcy drag) that couples the fluid and solid phases. This hydrodynamic force is linear in the fluid velocity only when the microscale inertia of the flow is weak, which is readily established in porous media whose microscale is of colloidal dimensions. The double-layer thickness (Debye length) is

$$\kappa^{-1}=\sqrt{kT\epsilon_s\epsilon_o/(2Ie^2)},$$

where $I=(1/2)\Sigma_{j=1}^{N}z_j^2n_j^\infty$ is the bulk ionic strength, with n_j^∞ the bulk ion concentrations. Since this work deals exclusively with steady (or quasisteady) flows, the fluid velocity in Eq. (5) is relative to a stationary polymer skeleton.

The equations are solved by perturbing (to linear order) from an equilibrium base state where $\boldsymbol{u}=\boldsymbol{0}$ and the equilibrium electrostatic potential, ion concentrations, and pressure are denoted ψ^0, n_j^0, and p^0, respectively [16,17]. With the application of a uniform electric field $\boldsymbol{E}$,

$$\psi=\psi^0+\psi', \quad n_j=n_j^0+n_j', \quad \boldsymbol{u}=\boldsymbol{u}',$$

where

$$\psi'=-\boldsymbol{E}\cdot\boldsymbol{r}+\hat{\psi}(r)\boldsymbol{E}\cdot\boldsymbol{e}_r, \quad n_j'=\hat{n}_j(r)\boldsymbol{E}\cdot\boldsymbol{e}_r,$$

and

$$\begin{aligned}\boldsymbol{u}&=\boldsymbol{\nabla}\times\boldsymbol{\nabla}\times f(r)\boldsymbol{E}\\&=-2f_rr^{-1}(\boldsymbol{E}\cdot\boldsymbol{e}_r)\boldsymbol{e}_r-(f_{rr}+f_rr^{-1})(\boldsymbol{E}\cdot\boldsymbol{e}_\theta)\boldsymbol{e}_\theta,\end{aligned} \tag{6}$$

which defines $f(r)$. Note that $f_r=\mathrm{d}f/\mathrm{d}r$ and $f_{rr}=\mathrm{d}^2f/\mathrm{d}r^2$; $\boldsymbol{r}$ is position in a spherical polar coordinate system (r,θ,ϕ) with unit basis vectors $(\boldsymbol{e}_r,\boldsymbol{e}_\theta,\boldsymbol{e}_\phi)$; and $\boldsymbol{e}_z$ is the orientation of the polar axis $(\boldsymbol{e}_r\cdot\boldsymbol{e}_z=\cos\theta)$.

At the particle-electrolyte interface ($r=a$),

$$\boldsymbol{u}=\boldsymbol{0} \quad \text{(no slip)}, \quad \boldsymbol{j}_j\cdot\boldsymbol{e}_r=0 \quad \text{(no flux)},$$

and

$$\epsilon_s\epsilon_o\boldsymbol{\nabla}_>\psi\cdot\boldsymbol{e}_r-\epsilon_p\epsilon_o\boldsymbol{\nabla}_<\psi\cdot\boldsymbol{e}_r = -\sigma \quad \text{(constant surface charge)},$$

where ϵ_p is the particle dielectric constant and σ is the (constant) surface charge density; the subscripts attached to the gradient operators distinguish the particle ($<$) and solvent ($>$) sides of the interface.

In the far field ($r\to\infty$),

$$\psi\to-\boldsymbol{E}\cdot\boldsymbol{r}+(\boldsymbol{E}\cdot\boldsymbol{e}_r)D^E r^{-2},$$

$$n_j\to n_j^\infty+(\boldsymbol{E}\cdot\boldsymbol{e}_r)C_j^E r^{-2},$$

$$\boldsymbol{u}\to-2C^E r^{-3}(\boldsymbol{E}\cdot\boldsymbol{e}_r)\boldsymbol{e}_r-C^E r^{-3}(\boldsymbol{E}\cdot\boldsymbol{e}_\theta)\boldsymbol{e}_\theta, \tag{7}$$

where the scalar coefficients D^E, C_j^E, and $C^E\eta/\ell^2$ are, respectively, the dipole strengths of the electrostatic potential, ion concentrations, and pressure perturbations, induced by the electric field. Note that the far-field flow is a Darcy flow, $\boldsymbol{u}=-(\ell^2/\eta)\boldsymbol{\nabla}p'$, whose *screened* velocity disturbance decays as r^{-3} as $r\to\infty$.

The full equations and boundary conditions above are the basis of an efficient numerical solution that yields the so-called asymptotic coefficients D^E, C_j^E, and C^E, which have been used to calculate the bulk *electrical conductivity* and *pore mobility* of dilute polymer-gel composites [5,18]. This work draws upon C^E, and introduces a new asymptotic coefficient Z^E to characterize the far-field decay of the electric-field-induced elastic displacement field.

B. Elastic deformation

Elastic deformation of the polymer gel is calculated by modeling the polymer skeleton as an elastic Brinkman medium, whose equation of static equilibrium is

$$\boldsymbol{\nabla}\cdot\boldsymbol{\sigma}+(\eta/\ell^2)\boldsymbol{u}=\boldsymbol{0}. \tag{8}$$

Here, the elastic stress tensor [19] is

$$\boldsymbol{\sigma}=\frac{\mathcal{E}}{(1+\nu)}\left(\boldsymbol{e}+\frac{\nu}{(1-2\nu)}(\boldsymbol{\nabla}\cdot\boldsymbol{v})\boldsymbol{\delta}\right), \tag{9}$$

where $\boldsymbol{v}$ is the (small-amplitude) displacement, $\mathcal{E}$ is Young's modulus, ν is Poisson's ratio, $\boldsymbol{e}=(1/2)[\boldsymbol{\nabla}\boldsymbol{v}+(\boldsymbol{\nabla}\boldsymbol{v})^T]$, and $\boldsymbol{\delta}$ is the identity tensor. The second-order tensor $\boldsymbol{\sigma}$ should not be confused with the surface charge density σ.

Substituting Eq. (9) into Eq. (8) gives

$$\frac{\mathcal{E}}{2(1+\nu)}\nabla^2\boldsymbol{v}+\frac{\mathcal{E}}{2(1+\nu)(1-2\nu)}\boldsymbol{\nabla}(\boldsymbol{\nabla}\cdot\boldsymbol{v})=-(\eta/\ell^2)\boldsymbol{u}, \tag{10}$$

where, again, the fluid velocity is relative to a stationary polymer skeleton ($\partial\boldsymbol{v}/\partial t=\boldsymbol{0}$).

When the (leading order) displacement is divergence free, which is the situation addressed throughout this paper, deformation can only influence the (isotropic) permeability tensor $(\ell^2/\eta)\boldsymbol{\delta}$ by inducing anisotropy. Note that any deformation-induced change in permeability yields a nonzero product of the permeability perturbation and the fluid velocity, the latter of which is itself a perturbation. Accordingly, these second-order terms are neglected in the present (linearized) theory.

There is also a possibility of anisotropy in permeability due to the underlying random microstructure of the medium (hydrogel matrix), which itself is not isotropic at very small length scales. However, we assume this medium to be statistically isotropic and homogeneous, so that, at the level of a representative volume element (RVE) of the deterministic continuum, the anisotropy vanishes just as the fluctuations in constitutive response tend to zero; see Ostoja-Starzewski and Wang [20] for a random elastic model. Such a scale-dependent homogenization (i.e., a passage from a random microstructure to the RVE) was recently studied in the context of Stokesian permeability [21], albeit the departure from anisotropy was not addressed explicitly; see also Ostoja-Starzewski [22] for related studies in many other material problems.

The Poisson ratios of several widely used, highly swollen, transparent hydrogels are reported greater than 0.45. In particular, poly(vinyl alcohol) hydrogels prepared with a mixed solvent of dimethyl sulfoxide and water have $\nu\approx0.472$ [23], and polyacrylamide hydrogels have $\nu\approx0.457$ [24]. However, it is important to note that these measurements are ascertained from macroscale experiments where the characteristic length and time scales cannot probe the equilibrium (long-time) state of strain. For example, the fractional change in volume after relaxing to equilibrium is $\delta V/L^3\sim(1-2\nu)l/L$, where the strain $l/L\ll1$ is the ratio of the imposed displacement l to the specimen size L. The flux of solvent flowing through the specimen during the so-called draining time τ is $u_c\sim\delta V/(L^2\tau)\sim(1-2\nu)l/\tau$. Further, the flux is driven by a pressure gradient $p_c/L\sim(\eta/\ell^2)u_c$, where, to balance the elastic stresses, the characteristic pressure is $p_c\sim\mathcal{E}(l/L)$. Together, the foregoing yield

$$\tau\sim(1-2\nu)(\eta/\mathcal{E})(L/\ell)^2, \tag{11}$$

so with $\eta\sim10^{-3}$ Pa s, $\mathcal{E}\sim10^5$ Pa, $L\sim10^{-2}$ m (macroscale experiment) and $\ell\sim10^{-9}$ m, the relaxation time is $\tau\sim(1-2\nu)10^6$ s. Clearly, this is extraordinarily long if ν is not sufficiently close to 0.5. Accordingly, when the experimental time scale (e.g., reciprocal frequency) is shorter than the draining time, the change in volume will be smaller than at equilibrium, and the apparent Poisson ratio will be greater than the drained value.

In contrast, the draining time associated with the displacement of a microsphere ($L=a\sim10^{-6}$ m) embedded in a hydrogel with $\mathcal{E}\sim10^5$ Pa and $\ell\sim10^{-9}$ m is only $\tau\sim(1-2\nu)10^{-2}$ s. Such an experiment is much better suited to probing the compressibility of the polymer skeleton. However, solving the problem with a compressible polymer matrix demands a distinctly different computational methodology than the one adopted in this paper. Moreover, compressibility is anticipated to yield *quantitative*—not qualitative—changes in the calculated particle displacement.

This expectation is supported, in part, by the fact that, in the absence of an electric field, the quasisteady particle displacement varies by at most 25% from the incompressible limit as Poisson's ratio spans the range 0–0.5 [25,26]. However, a definitive conclusion requires a solution of the electrokinetic equations with arbitrary Poisson's ratio; a goal that is beyond the relatively modest scope of the present work, but one that will be thoroughly addressed elsewhere.

Finally, the density and, hence, rigidity of the inclusions (e.g., polymer latex or silica) are typically much greater than those of the gel. Accordingly, the inclusions are treated as rigid spheres. Moreover, the displacement field is assumed to be continuous across the inclusion-hydrogel interface. Other interfacial conditions include the possibility of (tangential) slip (e.g., [27]) or an opening crack, for example. The opening of a crack significantly complicates the analysis, and a slipping boundary condition is difficult to justify here, since it requires a physical mechanism to exert an interfacial radial stress while maintaining zero (relative) radial displacement and zero tangential stress. Accordingly, neither possibility is pursued here.

III. SUPERPOSITION TO CALCULATE THE PARTICLE DISPLACEMENT

It is convenient to calculate the electric-field-induced particle displacement $\boldsymbol{Z}$ by superposing two linearly independent displacement fields.

One is the displacement field induced by a small displacement $\boldsymbol{Z}$ of the inclusion in the absence of an electric field ($\boldsymbol{E}=\boldsymbol{0}$). There is no Darcy drag, and the solution of Eq. (10) can be calculated analytically (see Appendix A). The resulting mechanical-contact force exerted by the polymer on the particle is [28]

$$\boldsymbol{f}^{m,Z} = -\frac{2\pi a\mathcal{E}\boldsymbol{Z}(1-\nu)}{(5/6-\nu)(1+\nu)}. \tag{12}$$

The other arises from the Darcy drag force when an electric field $\boldsymbol{E}$ is applied and the inclusion is fixed at the origin ($\boldsymbol{Z}=\boldsymbol{0}$). The Darcy drag force in Eq. (10) is calculated from the electrokinetic transport equations with a rigid polymer gel. Then the displacement can be obtained by solving Eq. (10). This is detailed in Sec. IV, where it is also shown that the mechanical-contact force exerted by the polymer on the inclusion is

$$\boldsymbol{f}^{m,E} = (8/3)\pi Z^E\mathcal{E}\boldsymbol{E} - 4\pi(\eta/\ell^2)C^E\boldsymbol{E}(\nu=0.5). \tag{13}$$

In addition to the net mechanical-contact force

$$\boldsymbol{f}^{m} = \boldsymbol{f}^{m,Z} + \boldsymbol{f}^{m,E}, \tag{14}$$

there are electrical and hydrodynamic (drag) forces acting on the particle, denoted $\boldsymbol{f}^{e,E}$ and $\boldsymbol{f}^{d,E}$, respectively. These are already known from earlier solutions of the electrokinetic transport equations with a rigid (unperturbed) polymer gel [5,15]. Their sum can be written in terms of the asymptotic coefficient C^E that characterizes the far-field decay of the electric-field-induced flow,

$$\boldsymbol{f}^{e,E} + \boldsymbol{f}^{d,E} = 4\pi(\eta/\ell^2)C^E\boldsymbol{E}. \tag{15}$$

Finally, static equilibrium of the particle demands

$$\boldsymbol{f}^{e,E} + \boldsymbol{f}^{d,E} + \boldsymbol{f}^{m,Z} + \boldsymbol{f}^{m,E} = \boldsymbol{0}. \tag{16}$$

Therefore, collecting the explicit expressions for the various forces above [Eqs. (12) and (13) (with $\nu=0.5$), and (15)] gives the particle displacement

$$\boldsymbol{Z} = (4/3)(Z^E/a)\boldsymbol{E} \quad (\nu=0.5). \tag{17}$$

The task of calculating Z^E is detailed in the next section. Note that the contributions involving C^E vanish, indicating that the slowest (r^{-1}) far-field decay of the displacement field vanishes upon superposition. In other words, there is no net force acting on the polymer, so the Darcy drag force exerted by the electrolyte on the polymer is counterbalanced by the mechanical-contact force exerted by the inclusion on the polymer. In a composite with a finite inclusion number density, or finite volume fraction ϕ, part of the net mechanical-contact force acting on the polymer must be provided by a mechanical support to balance an accompanying $O(\phi)$ average pressure gradient [5].

IV. ELECTRIC-FIELD-INDUCED MECHANICAL-CONTACT FORCE FOR AN INCOMPRESSIBLE, ELASTIC BRINKMAN MEDIUM

This section addresses the displacement induced by Darcy drag when an electric field is applied and the inclusion is fixed at the origin. This problem is adopted to calculate the force $\boldsymbol{f}^{m,E}$ appearing in Eq. (13). Note that the numerical solution is limited to incompressible ($\boldsymbol{\nabla}\cdot\boldsymbol{v}=0$) displacement fields, so $\nu=0.5$.

In Appendix B, the displacement field is expanded as a power series in a small parameter $\epsilon=1-2\nu$, i.e.,

$$\boldsymbol{v} = \boldsymbol{v}_0 + \epsilon\boldsymbol{v}_1 + \cdots. \tag{18}$$

The leading contribution to the displacement $\boldsymbol{v}_0$ is divergence free ($\boldsymbol{\nabla}\cdot\boldsymbol{v}_0=0$) and satisfies the $O(\epsilon)$ equation of static equilibrium,

$$\nabla^2\boldsymbol{v}_0 + \boldsymbol{\nabla}(\boldsymbol{\nabla}\cdot\boldsymbol{v}_1) = -(\eta/\ell^2)(3/\mathcal{E})\boldsymbol{u} \quad (\nu=0.5). \tag{19}$$

Note that $\boldsymbol{\nabla}\cdot\boldsymbol{v}_1$ is conventionally redefined as a pressure. Indeed, as shown in Appendix B, this quantity appears as an isotropic stress.

Incompressibility [as required by the $O(1)$ problem] is guaranteed by writing

$$\boldsymbol{v}_0 = \boldsymbol{\nabla}\times\boldsymbol{\nabla}\times g(r)\boldsymbol{E}, \tag{20}$$

where $g(r)$ is a function of radial position r. It follows that

$$\boldsymbol{v}_0 = -2g_r r^{-1}(\boldsymbol{E}\cdot\boldsymbol{e}_r)\boldsymbol{e}_r - (g_{rr}+g_r r^{-1})(\boldsymbol{E}\cdot\boldsymbol{e}_\theta)\boldsymbol{e}_\theta, \tag{21}$$

where, for example, $g_r = \mathrm{d}g/\mathrm{d}r$.

Because the fluid is also incompressible, its velocity field may be written as

$$\boldsymbol{u} = \boldsymbol{\nabla}\times\boldsymbol{\nabla}\times f(r)\boldsymbol{E}, \tag{22}$$

where $f(r)$ is available from earlier work examining the influence of an electric field [5] and a bulk concentration gradient [15] with a rigid polymer gel ($\boldsymbol{v}=\boldsymbol{0}$).

If the deformation is assumed not to affect electrokinetic transport processes, which is a reasonable approximation when the displacement is divergence free (so the polymer segment density and, hence, the Darcy permeability are unperturbed), then the earlier calculations also provide an exact solution with (weak) elastic deformation.

Substituting Eqs. (20) and (22) into the curl of Eq. (19) gives

$$\frac{\mathrm{d}}{\mathrm{d}r}\nabla^2\nabla^2 g + \frac{3\eta}{\mathcal{E}\ell^2}\frac{\mathrm{d}}{\mathrm{d}r}\nabla^2 f = 0, \tag{23}$$

where

$$\nabla^2 = \frac{1}{r^2}\frac{\mathrm{d}}{\mathrm{d}r}\left(r^2\frac{\mathrm{d}}{\mathrm{d}r}\right), \tag{24}$$

and $f(r)$ is known. In this manner, $\boldsymbol{v}_0$ is decoupled from $\boldsymbol{v}_1$.

The fourth-order ordinary differential equation for $g_r(r)$ is solved numerically as two second-order differential equations [29],

$$\frac{\mathrm{d}^2 h}{\mathrm{d}r^2} + \frac{4}{r}\frac{\mathrm{d}h}{\mathrm{d}r} - \frac{4}{r^2}h = -\frac{3\eta}{\mathcal{E}\ell^2}\left(\frac{\mathrm{d}^2 f_r}{\mathrm{d}r^2} + \frac{2}{r}\frac{\mathrm{d}f_r}{\mathrm{d}r} - \frac{2}{r^2}f_r\right), \tag{25}$$

$$\frac{\mathrm{d}^2 g_r}{\mathrm{d}r^2} = h. \tag{26}$$

When the displacement is continuous across the inclusion-hydrogel interface, and vanishes in the far field, the boundary conditions are

$$\boldsymbol{v}_0 = \boldsymbol{0} \quad \text{at} \quad r = a \tag{27}$$

and

$$\boldsymbol{v}_0 \to -2Z^E r^{-1}(\boldsymbol{E}\cdot\boldsymbol{e}_r)\boldsymbol{e}_r - Z^E r^{-1}(\boldsymbol{E}\cdot\boldsymbol{e}_\theta)\boldsymbol{e}_\theta \quad \text{as} \quad r \to \infty. \tag{28}$$

The asymptotic coefficient Z^E characterizes the strength of the r^{-1} decay of $\boldsymbol{v}$ (reflecting a net force). It follows that

$$g_r = g_{rr} = 0 \quad \text{at} \quad r = a \tag{29}$$

and

$$g_r \to Z^E \quad \text{and} \quad g_{rr} \to 0 \quad \text{as} \quad r \to \infty. \tag{30}$$

An analytical boundary-layer analysis that solves the problem when $\kappa a \gg 1$, $\ell \ll a$, and $|\zeta| < kT/e$ serves to verify the numerical solution and to highlight the parametric scaling of Z. The result is presented in Sec. V [Eq. (39)], where we also examine numerically exact solutions of the full model.

Turning to the force, the leading contribution to the isotropic stress requires knowledge of the $O(\epsilon)$ displacement field $\boldsymbol{v}_1$, which is not divergence free (see Appendix B). Clearly, the divergence of $\boldsymbol{v}_1$ is necessary to evaluate the leading contribution to the force. Fortunately, the isotropic stress can be obtained from the solution of the $O(\epsilon)$ problem above. This is achieved by integrating Eq. (B4) once $\boldsymbol{v}_0$ is known. The task is simplified even further, because only the far-field decay of the displacement and fluid velocity fields are needed to evaluate the force. We have verified our general procedure by applying it to two simpler problems: one is the classical problem of Stokes flow past a sphere, and the other is the elastic restoring force on a rigid sphere embedded in an incompressible elastic continuum. Recall, the exact solution of the latter problem, for any ν [see Eq. (12)], is worked out in Appendix A.

The mechanical-contact force exerted by the polymer on the inclusion is

$$\boldsymbol{f}^{m,E} = \int_{r=a} \boldsymbol{\sigma}\cdot\hat{\boldsymbol{n}}\,\mathrm{d}A = \int_{r\to\infty} \boldsymbol{\sigma}\cdot\hat{\boldsymbol{n}}\,\mathrm{d}A + \int_{r=a}^{\infty} (\eta/\ell^2)\boldsymbol{u}\,\mathrm{d}V. \tag{31}$$

Note that (see Appendix B)

$$\boldsymbol{\sigma} = \frac{2\mathcal{E}}{3}\left[\boldsymbol{e}_0 + \frac{1}{2}(\boldsymbol{\nabla}\cdot\boldsymbol{v}_1)\boldsymbol{\delta}\right], \tag{32}$$

where $\boldsymbol{e}_0 = (1/2)[\boldsymbol{\nabla}\boldsymbol{v}_0 + (\boldsymbol{\nabla}\boldsymbol{v}_0)^T]$, from Eq. (19),

$$\boldsymbol{\nabla}\cdot\boldsymbol{v}_1 = -\int_{\infty}^{r} [(\nabla^2\boldsymbol{v}_0) + (3/\mathcal{E})(\eta/\ell^2)\boldsymbol{u}]\cdot\boldsymbol{e}_r\,\mathrm{d}r \tag{33}$$

and

$$\begin{aligned}\boldsymbol{u} &= -2f_r r^{-1}(\boldsymbol{E}\cdot\boldsymbol{e}_r)\boldsymbol{e}_r - (f_{rr} + f_r r^{-1})(\boldsymbol{E}\cdot\boldsymbol{e}_\theta)\boldsymbol{e}_\theta \\ &\to -2C^E r^{-3}(\boldsymbol{E}\cdot\boldsymbol{e}_r)\boldsymbol{e}_r - C^E r^{-3}(\boldsymbol{E}\cdot\boldsymbol{e}_\theta)\boldsymbol{e}_\theta \quad \text{as} \quad r\to\infty.\end{aligned} \tag{34}$$

Recall, C^E is the asymptotic constant that represents the dipole strength of the far-field pressure field (decaying as r^{-2}) that drives the far-field Darcy flow (decaying as r^{-3}).

Evaluating the first integral on the right-hand side of Eq. (31) over the surface of a large concentric sphere gives

$$\int_{r\to\infty} \boldsymbol{\sigma}\cdot\hat{\boldsymbol{n}}\,\mathrm{d}A = (8/3)\pi Z^E\mathcal{E}\boldsymbol{E} - (4/3)\pi(\eta/\ell^2)C^E\boldsymbol{E} \quad (\nu = 0.5). \tag{35}$$

The volume integral can be transformed to another integral over the surface of a large concentric sphere [$\boldsymbol{\nabla}\cdot\boldsymbol{u} = 0$ and $\boldsymbol{u}(r=a) = \boldsymbol{0}$] giving

$$\begin{aligned}\int_{r=a}^{\infty} (\eta/\ell^2)\boldsymbol{u}\,\mathrm{d}V &= (\eta/\ell^2)\int_{r\to\infty} (\boldsymbol{x}\cdot\boldsymbol{u})\hat{\boldsymbol{n}}\,\mathrm{d}A \\ &= -(8/3)\pi(\eta/\ell^2)C^E\boldsymbol{E}.\end{aligned} \tag{36}$$

Finally, adding Eqs. (35) and (36) gives the mechanical-contact force as it appears in Eq. (13).

V. RESULTS

When solving the equations numerically, the characteristic scales adopted for length, velocity, and displacement are

$$\kappa^{-1}, u^* = \epsilon_s\epsilon_o(kT/e)^2/(\eta a) \quad \text{and} \quad \eta u^*/\mathcal{E} = \epsilon_s\epsilon_o(kT/e)^2/(\mathcal{E}a),$$

respectively. It is therefore convenient to introduce a dimensionless asymptotic coefficient $\hat{Z}^E$ so

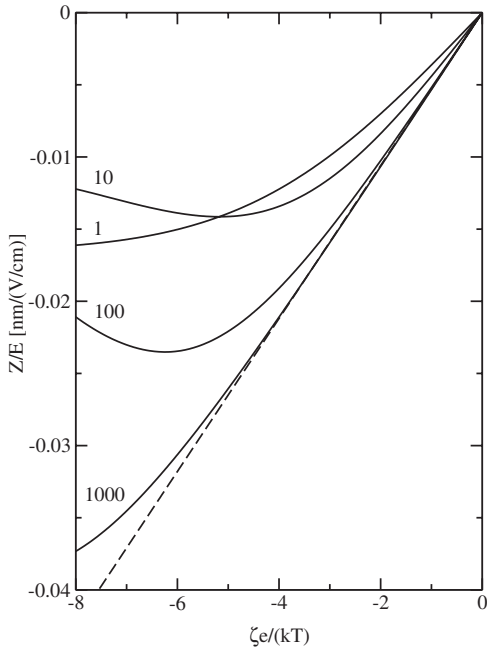

FIG. 2. The ratio of the displacement Z (nm) to the electric field strength E (V cm^{-1}) as a function of the scaled ζ potential $\zeta e/(kT)$ for various scaled reciprocal double-layer thicknesses $\kappa a=1$, 10, 100, and 1000: NaCl at $T=298$ K; $a=500$ nm; $\ell=5$ nm; $\mathcal{E}=1$ kPa; $\nu=0.5$. Note that the displacement is inversely proportional to Young's modulus $\mathcal{E}$. The dashed line is the boundary-layer theory [Eq. (39)].

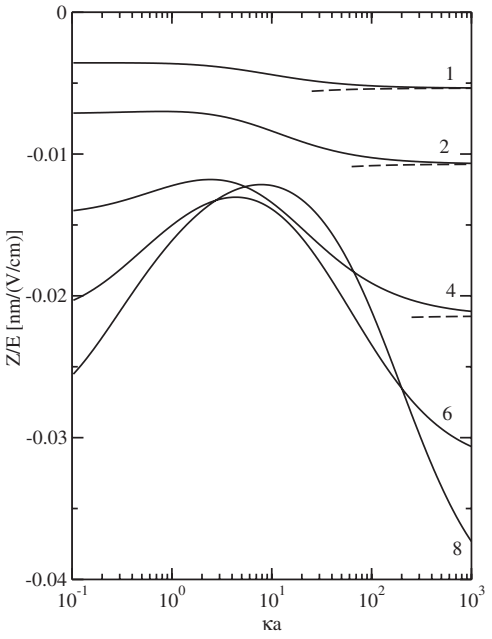

FIG. 3. The ratio of the displacement Z (nm) to the electric field strength E (V cm^{-1}) as a function of the scaled reciprocal double-layer thickness κa for various scaled ζ potentials $-\zeta e/(kT)=1$, 2, 4, 6, and 8: NaCl at $T=298$ K; $a=500$ nm; $\ell=5$ nm; $\mathcal{E}=1$ kPa; $\nu=0.5$. Note that the displacement is inversely proportional to Young's modulus $\mathcal{E}$. The dashed lines are the boundary-layer theory [Eq. (39)].

$$Z^E = \frac{\epsilon_s \epsilon_o (kT/e) a}{\mathcal{E}(\kappa a)^2} \hat{Z}^E. \tag{37}$$

Accordingly, the particle displacement [Eq. (17)] is

$$\boldsymbol{Z} = (4/3) \frac{\epsilon_s \epsilon_o (kT/e)}{\mathcal{E}(\kappa a)^2} \hat{Z}^E \boldsymbol{E}. \tag{38}$$

The independent dimensionless parameters adopted below are κa, $\zeta e/(kT)$, and $\kappa \ell$. Note that $\hat{Z}^E$ is independent of $\mathcal{E}$, and, furthermore, we will see that the displacement is a very weak function of ℓ. Using a boundary-layer approximation for C^E [18], an analytical solution for Z^E, when $\kappa a \gg 1$, $\ell \ll a$, and $|\zeta| < kT/e$, yields

$$\boldsymbol{Z} \to 3\zeta \epsilon_s \epsilon_o \mathcal{E}^{-1} \boldsymbol{E} \quad \text{as} \quad \kappa a \to \infty, \tag{39}$$

which is the counterpart to Eq. (2) identified in the introduction.

A. Particle displacement with NaCl electrolytes

To draw a closer connection to experiments, Z/E is plotted in Figs. 2 and 3 with $\mathcal{E}=1$ kPa. Therefore, actual displacements Z (nm) can be conveniently obtained by multiplying the ordinates by the electric field strength E (V cm^{-1}) and dividing by Young's modulus $\mathcal{E}$ (kPa).

Figure 2 shows Z/E as a function of the scaled ζ potential $\zeta e/(kT)$ for a particle with radius $a=500$ nm and a hydrogel with Young's modulus $\mathcal{E}=1$ kPa ($\nu=0.5$) and Brinkman screening length $\ell=5$ nm. The electrolyte is NaCl, with ionic strengths corresponding to $\kappa a=1-10^3$. As expected, the (negative) particle displacement is in the direction of the electrical force, $4\pi a^2 \sigma \boldsymbol{E}$, and increases with the magnitude of the ζ potential ($\zeta<0$).

At low ζ potentials, the displacement is clearly proportional to $|\zeta|$ and, hence, the surface charge density $\sigma=\epsilon_s \epsilon_o \kappa \zeta$ (when $|\zeta|<kT/e$). As expected, the numerical solutions approach the boundary-layer theory [Eq. (39)] as $\kappa a \to \infty$. However, the numerical results reveal distinct maximums at moderate and large values of $|\zeta|$; these are due to polarization of the diffuse double layer. As is well known from electrophoresis (e.g., [16]), polarization diminishes the local electric field, thereby attenuating the electrical force. Because polarization by electromigration and relaxation by molecular diffusion are practically independent of the polymer gel in this model [5], they are as significant here as they are in electrophoresis.

Figure 3 shows Z/E under the same conditions as in Fig. 2, but now as a function of the scaled reciprocal double-layer thickness κa, with each curve corresponding to a constant ζ potential. The displacement is clearly a weak function of κa, particularly when $|\zeta|$ is small, and, as expected from Fig. 2, a much stronger function of ζ. Clearly, this way of presenting the results emphasizes the large values of κa required for the boundary-layer theory to be accurate.

Since Figs. 2 and 3 are presented with a fixed value of $\ell/a=0.01$, it remains to establish the influence of the Darcy permeability (or Brinkman screening length). Recall, the boundary-layer theory [Eq. (39)] indicates that the displace-

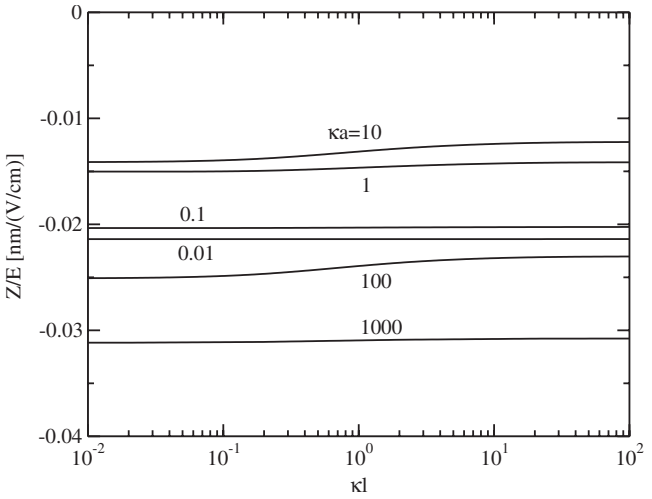

FIG. 4. The ratio of the displacement Z (nm) to the electric field strength E (V cm^{-1}) as a function of the scaled Brinkman screening length $\kappa\ell$ with $\zeta e/(kT)=-6$ and $\kappa a=0.01$, 0.1, 1, …, 1000: KCl at $T=298$ K; $a=500$ nm; $\mathcal{E}=1$ kPa; $\nu=0.5$. Note that the displacement is inversely proportional to Young's modulus $\mathcal{E}$.

ment is independent of ℓ. More generally, however, the particle displacement reflects the far-field electric-field-induced distortion of the polymer skeleton when the particle is fixed at the origin by an external force

$$\boldsymbol{f}^E = -\boldsymbol{f}^{d,E} - \boldsymbol{f}^{e,E} - \boldsymbol{f}^{m,E} = -(8/3)\pi Z^E \mathcal{E}\boldsymbol{E}. \tag{40}$$

Figure 4 shows how the particle displacement varies over 4 decades of the scaled Brinkman screening length $\kappa\ell$ when $\zeta e/(kT)=-6$ and $\kappa a=10^{-2}-10^3$. While there are obvious transitions when $\kappa\ell\sim 1$ (from plateaus where $\kappa\ell\to 0$ and ∞), the displacement is remarkably insensitive to ℓ.

In the next section, we identify a simple transformation that permits Z^E and, hence, the particle displacement, to be approximated by the well-known electrophoretic mobility, which, of course, is independent of ℓ. Accordingly, we write

$$\boldsymbol{Z} = 3\zeta\epsilon_s\epsilon_o\mathcal{E}^{-1} f[\kappa a, \zeta e/(kT), \kappa\ell]\boldsymbol{E}, \tag{41}$$

where the dimensionless function

$$f[\kappa a, \zeta e/(kT), \kappa\ell] = \frac{4\hat{Z}^E[\kappa a, \zeta e/(kT), \kappa\ell]}{9(\kappa a)^2 \zeta e/(kT)} \tag{42}$$

and, to a reasonable approximation,

$$f[\kappa a, \zeta e/(kT), \kappa\ell] \approx f[\kappa a, \zeta e/(kT), \infty]. \tag{43}$$

It follows that Fig. 2 or Fig. 3 is sufficient to span a significant range of the parameter space (strictly for negatively charged inclusions and NaCl electrolyte). Furthermore, from Eqs. (2) and (39), it is evident that $f\to 2/3$ as $\kappa a\to 0$ (with $|\zeta|<kT/e$) and $f\to 1$ as $\kappa a\to\infty$.

B. Connection to the electrophoretic mobility

The displacements shown in Figs. 2 and 3 bear a close resemblance to the electrophoretic mobility [16], so we present in Figs. 5 and 6 a *scaled displacement*

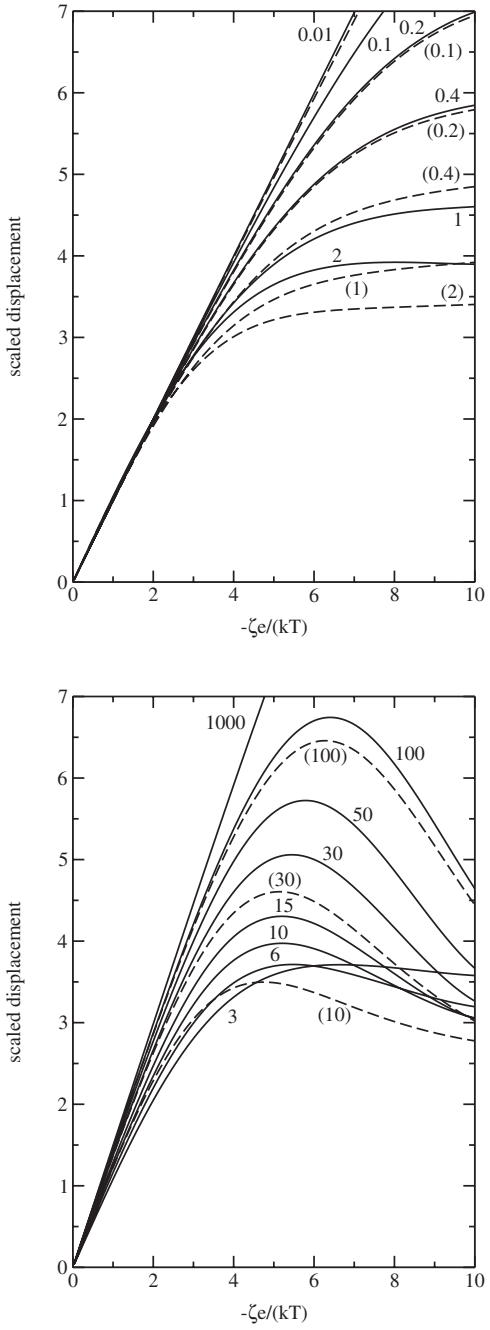

FIG. 5. The scaled displacement $-(Z/E)\mathcal{E}e/(2\epsilon_s\epsilon_o kT)$ as a function of the scaled ζ potential $-\zeta e/(kT)$ for various scaled reciprocal double-layer thicknesses $\kappa a=0.01$, 0.1, 0.2, 0.4, 1, and 2 (solid lines, top panel); and $\kappa a=3$, 6, 10, 15, 30, 50, 100, and 1000 (solid lines, bottom panel): KCl at $T=298$ K; $a=500$ nm; $\ell=5$ nm; $\nu=0.5$. Dashed lines are the scaled electrophoretic mobility $(U/E)3\eta e/(2\epsilon_s\epsilon_o kT)$ for selected values (labels in parentheses) of $\kappa a=0.01$, 0.1, 0.2, 0.4, 1, and 2 (top panel); and 10, 30, and 100 (bottom panel).

$$(Z/E)\mathcal{E}e/(2\epsilon_s\epsilon_o kT) = (3/2) f[\kappa a, \zeta e/(kT), \kappa\ell]\zeta e/(kT) \tag{44}$$

for a symmetrical electrolyte (KCl) (solid lines, Fig. 5) and a representative asymmetric electrolyte [$Ba(NO_3)_2$] (Fig. 6).

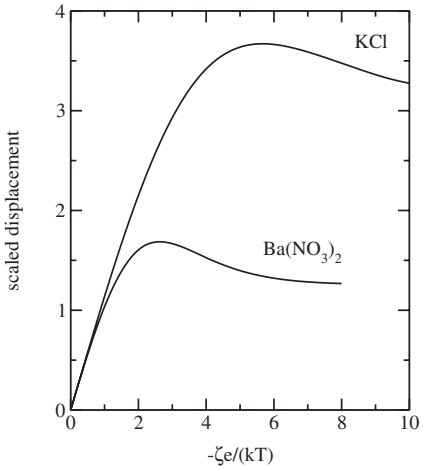

FIG. 6. The scaled displacement $-(Z/E)\mathcal{E}e/(2\epsilon_s\epsilon_o kT)$ as a function of the scaled ζ potential $-\zeta e/(kT)$ for scaled reciprocal double-layer thickness $\kappa a=5$: KCl and $Ba(NO_3)_2$ at $T=298$ K; $a=500$ nm; $\ell=5$ nm; $\nu=0.5$.

This dimensionless quantity (solid lines) has a very similar dependence on κa and $\zeta e/(kT)$ as the *scaled electrophoretic mobility* (dashed lines)

$$(U/E)3\eta e/(2\epsilon_s\epsilon_o kT) \tag{45}$$

presented in the well-known paper by O'Brien and White (see [16], also see their Figs. 3, 4, and 6) [30]. Here, U is the electrophoretic velocity, i.e., the translational velocity acquired by a charged spherical colloid dispersed in a Newtonian electrolyte in response to a (weak) electric field E.

The difference between the scaled mobility and scaled displacement highlighted in Fig. 5 is small when $|\zeta|<kT/e$, but increases appreciably when $\kappa a\sim 1$ and $|\zeta|>3kT/e$. Note that the scaled mobility is smaller than the respective scaled displacement, because the electrophoresis problem overestimates the convective contribution to the ion fluxes, thereby over-polarizing the diffuse double layer and, therefore, underestimating the electrical force in the particle-displacement problem.

A simple but approximate relationship between Z/E and U/E can be established by eliminating the Darcy drag force from the fluid momentum equation [Eq. (5)] and the polymer equation of static equilibrium [Eq. (10)]. More specifically, adding Eqs. (5) and (10) produces the momentum conservation equation in the electrophoresis problem [i.e., Eq. (5) without the Darcy drag term] with a modified fluid velocity

$$\boldsymbol{u}' = \boldsymbol{u} + \boldsymbol{v}\mathcal{E}/(3\eta). \tag{46}$$

Recall, $\boldsymbol{u}$ is the fluid velocity in the polymer gel and $\boldsymbol{v}$ is the displacement of the skeleton.

By setting $\boldsymbol{u}=\boldsymbol{u}'$ in the ion conservation equation, the solution of the electrophoresis problem (involving only $\boldsymbol{u}'$) overestimates the convective ion fluxes by an $O[(v_c/u_c)\mathcal{E}/(3\eta)]$ amount; here, v_c and u_c are, respectively, characteristic polymer displacement and fluid velocity scales. However, since the convective ion fluxes are $O(\mathrm{Pe}_j)$, where the Péclet numbers $\mathrm{Pe}_j=u_c\kappa^{-1}/D_j\ll 1$, the absolute errors are small.

Note that the polymer displacement reflects a transfer of the electrical body force from the fluid to the elastic skeleton. This transfer occurs by direct coupling of the fluid and polymer (via the Darcy drag force) and through indirect coupling by the transfer of viscous stresses from the fluid to the particle, which, in turn, are transferred to the polymer via mechanical contact between the particle and polymer. Consequently, the polymer distortion must be independent of the permeability in so far as the electrical body force is constant. However, the electrically driven flow increases significantly with the permeability (either as ℓ or ℓ^2, depending on κ^{-1} [5,18]), so the $O[(v_c/u_c)\mathcal{E}/(3\eta)]$ errors in the ion conservation equations must diminish with increasing permeability. Accordingly, the solution of the electrophoresis problem must yield an increasingly accurate solution of the particle displacement problem as $\kappa\ell\to\infty$.

More quantitatively, the solution of the (E) electrophoresis problem [16] yields $u'\sim\bar{C}^E Er^{-1}$ as $r\to\infty$. Therefore, because $v\sim Z^E Er^{-1}$ and $u\sim C^E Er^{-3}$ as $r\to\infty$, it follows from Eq. (46) that

$$Z^E\to\bar{C}^E 3\eta/\mathcal{E} \quad \text{as} \quad \kappa\ell\to\infty \quad (\nu=0.5). \tag{47}$$

Furthermore, since the electrophoretic mobility

$$M\equiv U/E=\bar{C}^E/\bar{C}^U, \tag{48}$$

where $\bar{C}^E$ and $\bar{C}^U$ are the asymptotic coefficients associated with the far-field decay of the fluid velocity in the (E) and (U) (electrophoresis) problems [16], Eqs. (17), (47), and (48) give

$$\boldsymbol{Z}\to F(3\eta/\mathcal{E})M\boldsymbol{E} \quad \text{as} \quad \kappa\ell\to\infty \quad (\nu=0.5). \tag{49}$$

Note that $F=(4/3)\bar{C}^U/a=D_s/D\sim 1$ is the particle *drag coefficient*, which can be conveniently expressed as the ratio of the *Stokes-Einstein-Sutherland* diffusivity [31,32] $D_s=kT/(6\pi\eta a)$ to the actual diffusivity $D[\kappa a,\zeta e/(kT)]\geq D_s$. The drag coefficient is shown in Fig. 7 for negatively charged colloidal spheres in a KCl electrolyte. Since $1\leq F<1.2$ and most often $1\leq F\lesssim 1.02$, the error in the particle displacement that comes from setting $F=1$ in Eq. (49) tends to be small compared to the error arising from finite $\kappa\ell$.

To demonstrate the correctness of Eq. (49), let us briefly consider a specific example where $\zeta e/(kT)=-6$ and $\kappa a=10$. From Fig. 4, the scaled displacements are ≈ 3.89 and ≈ 3.42 when $\kappa\ell=0.1$ and $\kappa\ell\to\infty$, respectively. Furthermore, from Fig. 5, the scaled mobility and drag coefficient are ≈ 3.36 and ≈ 1.016, respectively. Therefore, multiplying the scaled mobility by the drag coefficient gives ≈ 3.41, which, as expected, compares extremely well with the value (≈ 3.42) obtained directly when $\kappa\ell\gg 1$.

We have therefore established that the electrophoretic mobility and drag coefficient combine [as indicated in Eq. (49)] to yield the correct limiting value of the scaled particle displacement as $\kappa\ell\to\infty$. Furthermore, the difference between

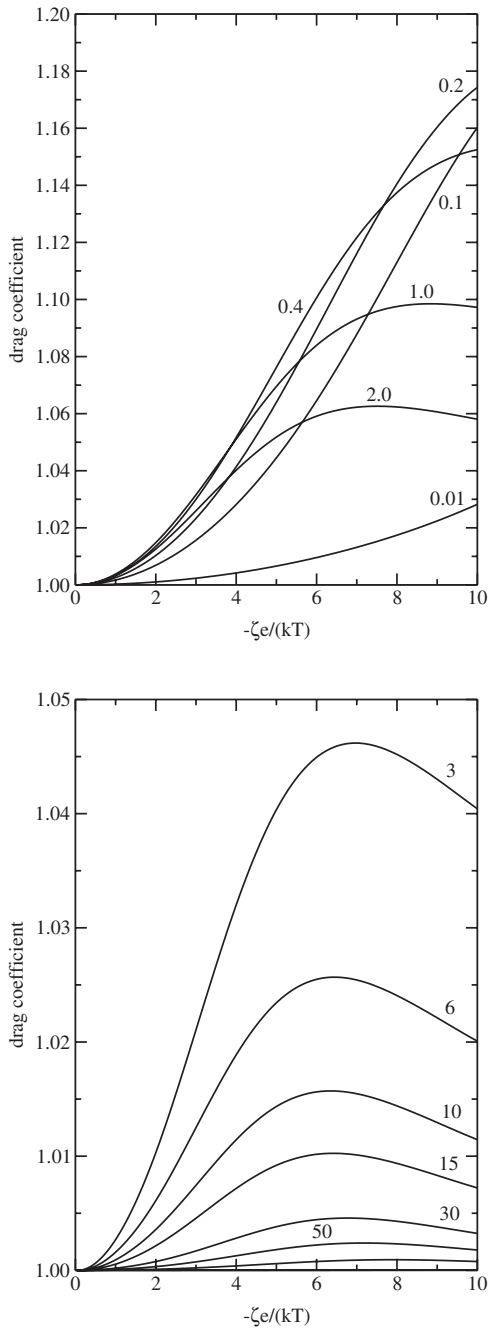

FIG. 7. The drag coefficient $F=(4/3)\bar{C}^U/a=D_s/D[\kappa a,\zeta e/(kT)]$ for charged spherical colloids as a function of the scaled ζ potential $-\zeta e/(kT)$ for various scaled reciprocal double-layer thicknesses $\kappa a=0.01$, 0.1, 0.2, 0.4, 1, and 2 (top panel); and $\kappa a=3$, 6, 10, 15, 30, 50, 100, and 1000 (bottom panel): KCl at $T=298$ K.

the displacement with impenetrable and infinitely permeable polymer reflects the degree to which polymer influences convective ion transport. Finally, because polarization by convection is weak relative to electromigrative polarization and diffusive relaxation, the influence of permeability on the displacement is generally small. It should be noted, however, that Young's modulus (or shear modulus) of the skeleton and the permeability both vary with the polymer density according to scaling laws that have been studied extensively in the polymer physics literature (e.g., [33]). In practice, therefore, particle displacements are expected to vary primarily with the modulus, with relatively insignificant changes due to the accompanying change in permeability.

VI. SUMMARY

We presented a theoretical model to calculate the electric-field-induced displacement of a charged, spherical colloid embedded in an electrolyte-saturated polymer gel. The standard electrokinetic model describes electric-field-induced transport of ions and electrolyte momentum, with a Darcy-drag term that couples the electrolyte mass and momentum conservation equations (Brinkman's equations) to a continuum equation of static equilibrium for an unbounded, incompressible, linearly elastic polymer skeleton.

The scaled particle displacement

$$(Z/E)\mathcal{E}e/(2\epsilon_s\epsilon_o kT)$$

has a similar dependence on $\zeta e/(kT)$ and κa as the well-known scaled electrophoretic mobility

$$(U/E)3\eta e(2\epsilon_s\epsilon_o kT).$$

More precisely, we showed that the product of the scaled electrophoretic mobility and particle drag (friction) coefficient yields the exact scaled displacement when $\kappa\ell\to\infty$ (i.e., when the polymer skeleton presents zero hydrodynamic resistance to flow). However, because the particle displacement decreases only slightly as $\kappa\ell$ passes through ~ 1, when increasing from 0 to ∞, the scaled electrophoretic mobility provides an excellent approximation of the scaled displacement over a wide range of the experimentally accessible parameter space. Therefore, as expected from electrophoresis, the scaled displacement is linear in the ζ potential when $|\zeta|\lesssim 2kT/e$, and has distinct maximums when $|\zeta|\sim 5kT/e$. The decrease in displacement with increasing ζ potential is due to polarization and relaxation of the diffuse double layer. Evidently, polarization is dominated by electromigration, since the influence of convection, which can be completely arrested by a hydrodynamically impenetrable polymer skeleton, is extremely weak.

We did not examine the stresses in the surrounding polymer. Nevertheless, our calculations provide an important first step toward future studies aimed at quantifying the microscale states of stress (and strain) when these soft composite materials are subjected to electric fields. Our model may be helpful for studying fracture, and it provides a means of quantitatively interpreting experiments designed to measure small electric-field-induced displacements of charged inclusions. In turn, these could be used to probe the mechanics of weak (uncharged) polymer gels at length and time scales that are beyond the reach of conventional (macroscale) rheometers.

ACKNOWLEDGMENTS

One of the authors (R.J.H.) gratefully acknowledges support from the Natural Sciences and Engineering Research

Council of Canada (NSERC) (Grant No. 204542) and the Canada Research Chairs program (Tier II).

APPENDIX A: FORCE TO DISPLACE A FINITE SIZED SPHERE EMBEDDED IN A COMPRESSIBLE ELASTIC CONTINUUM

This appendix provides an analytical solution of the equation of static equilibrium in the absence of body forces (Darcy drag). In turn, the force required to displace (by distance $\mathbf{Z}$) a rigid sphere (with radius a) embedded in an unbounded elastic continuum (with Young's modulus $\mathcal{E}$ and Poisson's ratio ν) is obtained.

Substituting a solution of the form

$$\boldsymbol{v} = \boldsymbol{v}_0 + \boldsymbol{v}_1, \tag{A1}$$

where

$$\nabla^2 \boldsymbol{v}_0 = \mathbf{0}, \tag{A2}$$

into the equation of static equilibrium [Eq. (10)] gives

$$\nabla^2 \boldsymbol{v}_1 + \frac{1}{(1-2\nu)} \nabla [\nabla \cdot (\boldsymbol{v}_0 + \boldsymbol{v}_1)] = \mathbf{0}. \tag{A3}$$

Taking the curl yields

$$\nabla^2 (\nabla \times \boldsymbol{v}_1) = 0, \tag{A4}$$

which, with the prevailing axial symmetry, provides a scalar equation for $(\nabla \times \boldsymbol{v}_1) \cdot \boldsymbol{e}_\phi$. Since $\nabla \times \boldsymbol{v}_1$ is an harmonic pseudovector, symmetry and linearity yield a nonzero decaying solution $\nabla \times \boldsymbol{v}_1 \sim \mathbf{Z} \times \nabla r^{-1}$. It follows that $\boldsymbol{v}_1 \sim \mathbf{Z} r^{-1}$, which is harmonic and, hence, can be attributed to $\boldsymbol{v}_0$. Accordingly, the only nonharmonic contribution to $\boldsymbol{v}_1$ is irrotational $(\nabla \times \boldsymbol{v}_1 = \mathbf{0})$ and, hence,

$$\boldsymbol{v}_1 = \nabla \phi, \tag{A5}$$

where ϕ is a scalar function of position. Substituting this into Eq. (A3) gives

$$\nabla [\nabla \cdot \boldsymbol{v}_0 + 2(1-\nu) \nabla^2 \phi] = \mathbf{0}, \tag{A6}$$

so

$$\nabla \cdot \boldsymbol{v}_0 + 2(1-\nu) \nabla^2 \phi = 0. \tag{A7}$$

Again, symmetry and linearity considerations yield the general decaying solution

$$\boldsymbol{v}_0 = c_0 \mathbf{Z} + c_1 \mathbf{Z} r^{-1} + c_2 (\mathbf{Z} \cdot \nabla) \nabla (r^{-1}). \tag{A8}$$

It follows that

$$\nabla \cdot \boldsymbol{v}_0 = c_1 \mathbf{Z} \cdot \nabla (r^{-1}) \quad (= -c_1 \mathbf{Z} \cdot \boldsymbol{e}_r r^{-2}) \tag{A9}$$

and, hence,

$$\nabla^2 \phi = -\frac{c_1 \mathbf{Z} \cdot \nabla (r^{-1})}{2(1-\nu)}. \tag{A10}$$

Note that $\nabla^2 \psi = r^{-1}$ has the solution $\psi = r/2$, so writing Eq. (A10) as

$$\nabla^2 \phi = -\frac{c_1 \mathbf{Z} \cdot \nabla (\nabla^2 \psi)}{2(1-\nu)} \tag{A11}$$

requires

$$\phi = -\frac{c_1 \mathbf{Z} \cdot \boldsymbol{e}_r}{4(1-\nu)} \tag{A12}$$

and, hence,

$$\boldsymbol{v}_1 = \nabla \phi = -\frac{c_1}{4r(1-\nu)} [\mathbf{Z} - (\mathbf{Z} \cdot \boldsymbol{e}_r) \boldsymbol{e}_r]. \tag{A13}$$

Finally, the complete displacement field is

$$\boldsymbol{v} = c_0 \mathbf{Z} + \frac{c_1}{r} \mathbf{Z} - \frac{c_1}{4r(1-\nu)} [\mathbf{Z} - (\mathbf{Z} \cdot \boldsymbol{e}_r) \boldsymbol{e}_r] + \frac{c_2}{r^3} [3(\mathbf{Z} \cdot \boldsymbol{e}_r) \boldsymbol{e}_r - \mathbf{Z}], \tag{A14}$$

where the scalar constants c_0, c_1, and c_2 must be chosen to satisfy the boundary conditions.

1. No-slip boundary condition

If, for example, $\boldsymbol{v} \to -\mathbf{Z}$ as $r \to \infty$ and $\boldsymbol{v} = \mathbf{0}$ at $r = a$ (fixed), then $c_0 = -1$ and

$$\mathbf{0} = -\mathbf{Z} + \frac{c_1}{a} \mathbf{Z} + \frac{c_2}{a^3} [3(\mathbf{Z} \cdot \boldsymbol{e}_r) \boldsymbol{e}_r - \mathbf{Z}] - \frac{c_1}{4a(1-\nu)} [\mathbf{Z} - (\mathbf{Z} \cdot \boldsymbol{e}_r) \boldsymbol{e}_r], \tag{A15}$$

which requires

$$c_1 = \frac{6(1-\nu)a}{(5-6\nu)} \quad \text{and} \quad c_2 = \frac{a^3}{2(6\nu-5)}. \tag{A16}$$

The mechanical-contact force on the inclusion is therefore

$$\boldsymbol{f}^m = \int_{r=a} \boldsymbol{\sigma} \cdot \hat{\boldsymbol{n}} \, \mathrm{d}A = -\frac{2\pi \mathcal{E} c_1 \mathbf{Z}}{(1+\nu)} = -\frac{12\pi \mathcal{E} a \mathbf{Z} (1-\nu)}{(5-6\nu)(1+\nu)}. \tag{A17}$$

Note that the displacement field can be rewritten in terms of the force, so the Green's function

$$\boldsymbol{G} = \frac{(1+\nu)}{8\pi \mathcal{E}(1-\nu) r} [(3-4\nu) \boldsymbol{\delta} + \boldsymbol{e}_r \boldsymbol{e}_r] \tag{A18}$$

is obtained by changing reference frames ($\boldsymbol{v} = \mathbf{Z}$ at $r = a$, and $\boldsymbol{v} \to \mathbf{0}$ as $r \to \infty$) and letting $a \to 0$.

2. Slip boundary condition

Again, if $\boldsymbol{v} \to -\mathbf{Z}$ as $r \to \infty$, but $\boldsymbol{v} \cdot \boldsymbol{e}_r = 0$ at $r = a$ (zero radial displacement) and $\boldsymbol{\sigma} \cdot \boldsymbol{e}_r - (\boldsymbol{\sigma} \cdot \boldsymbol{e}_r) \cdot \boldsymbol{e}_r \boldsymbol{e}_r = \mathbf{0}$ at $r = a$ (zero tangential stress), then $c_0 = -1$, and

$$c_1 = \frac{6(1-\nu)a}{(7-8\nu)} \quad \text{and} \quad c_2 = \frac{(1-2\nu)a^3}{2(7-8\nu)}. \tag{A19}$$

The mechanical-contact force (on the inclusion) is then

$$\boldsymbol{f}^m = -\frac{2\pi \mathcal{E} c_1 \mathbf{Z}}{(1+\nu)} = -\frac{12\pi \mathcal{E} a \mathbf{Z} (1-\nu)}{(7-8\nu)(1+\nu)}. \tag{A20}$$

APPENDIX B: LEADING-ORDER ISOTROPIC STRESS FOR AN INCOMPRESSIBLE ELASTIC CONTINUUM

Writing the displacement field as

$$\boldsymbol{v} = \boldsymbol{v}_0 + \epsilon \boldsymbol{v}_1 + \epsilon^2 \boldsymbol{v}_2 + \cdots, \tag{B1}$$

where $\epsilon = (1-2\nu) \ll 1$, substituting this into the equation of static equilibrium

$$\nabla^2 \boldsymbol{v} + \frac{1}{\epsilon} \boldsymbol{\nabla} (\boldsymbol{\nabla} \cdot \boldsymbol{v}) = -(\eta/\ell^2) \boldsymbol{u} \frac{(3-\epsilon)}{\mathcal{E}}, \tag{B2}$$

and collecting terms of like order in ϵ gives at $O(1)$,

$$\boldsymbol{\nabla}(\boldsymbol{\nabla} \cdot \boldsymbol{v}_0) = \boldsymbol{0}; \tag{B3}$$

at $O(\epsilon)$,

$$\nabla^2 \boldsymbol{v}_0 + \boldsymbol{\nabla}(\boldsymbol{\nabla} \cdot \boldsymbol{v}_1) = -(\eta/\ell^2) \boldsymbol{u} \frac{3}{\mathcal{E}}; \tag{B4}$$

at $O(\epsilon^2)$,

$$\nabla^2 \boldsymbol{v}_1 + \boldsymbol{\nabla}(\boldsymbol{\nabla} \cdot \boldsymbol{v}_2) = (\eta/\ell^2) \boldsymbol{u} \frac{1}{\mathcal{E}}; \tag{B5}$$

and at $O(\epsilon^3)$,

$$\nabla^2 \boldsymbol{v}_2 + \boldsymbol{\nabla}(\boldsymbol{\nabla} \cdot \boldsymbol{v}_3) = \boldsymbol{0}. \tag{B6}$$

Note that, if $\boldsymbol{u}$ and $\boldsymbol{v}_0$ are both divergence-free, then $\boldsymbol{\nabla} \cdot \boldsymbol{v}_1$, $\boldsymbol{\nabla} \cdot \boldsymbol{v}_2$, etc., all satisfy Laplace's equation with general solution, e.g., $\boldsymbol{\nabla} \cdot \boldsymbol{v}_1 = a_1 + b_1 \boldsymbol{E} \cdot \boldsymbol{\nabla} r^{-1}$.

Because the leading contribution to the displacement $\boldsymbol{v}_0$ is divergence free [Eq. (B3)], it can be written as

$$\boldsymbol{v}_0 = \boldsymbol{\nabla} \times \boldsymbol{\nabla} \times g(r) \boldsymbol{E}. \tag{B7}$$

Substituting this into the curl of Eq. (B4) gives

$$\frac{\mathrm{d}}{\mathrm{d}r} \nabla^2 \nabla^2 g + \frac{3\eta}{\mathcal{E}\ell^2} \frac{\mathrm{d}}{\mathrm{d}r} \nabla^2 f = 0, \tag{B8}$$

where

$$\nabla^2 = \frac{1}{r^2} \frac{\mathrm{d}}{\mathrm{d}r} \left(r^2 \frac{\mathrm{d}}{\mathrm{d}r} \right) \tag{B9}$$

and $f(r)$ is known. Clearly, the solution is independent of $\boldsymbol{v}_1$. Note, however, that $\boldsymbol{v}_1$ contributes to the leading-order stress,

$$\boldsymbol{\sigma}_0 = \frac{2\mathcal{E}}{3} \left[\boldsymbol{e}_0 + \frac{1}{2} (\boldsymbol{\nabla} \cdot \boldsymbol{v}_1) \boldsymbol{\delta} \right], \tag{B10}$$

where $\boldsymbol{e}_0 = (1/2)[\boldsymbol{\nabla} \boldsymbol{v}_0 + (\boldsymbol{\nabla} \boldsymbol{v}_0)^T]$. It follows that the leading contribution to the integral of the surface traction is

$$\boldsymbol{f}_0' = \frac{\mathcal{E}}{3} \int_{r \to \infty} [\boldsymbol{\nabla} \boldsymbol{v}_0 + (\boldsymbol{\nabla} \boldsymbol{v}_0)^T + (\boldsymbol{\nabla} \cdot \boldsymbol{v}_1) \boldsymbol{\delta}] \cdot \boldsymbol{e}_r \mathrm{d}A, \tag{B11}$$

where [Eq. (B4)]

$$\boldsymbol{\nabla} \cdot \boldsymbol{v}_1 = -\int_{\infty}^{r} \left((\eta/\ell^2) \boldsymbol{u} \frac{3}{\mathcal{E}} + \nabla^2 \boldsymbol{v}_0 \right) \cdot \boldsymbol{e}_r \mathrm{d}r'. \tag{B12}$$

Note that only the far-field decays of $\boldsymbol{u}$ and $\boldsymbol{v}_0$ are necessary to evaluate this integral when $r \to \infty$. Recall,

$$\boldsymbol{u} \to -2C^E r^{-3} (\boldsymbol{E} \cdot \boldsymbol{e}_r) \boldsymbol{e}_r - C^E r^{-3} (\boldsymbol{E} \cdot \boldsymbol{e}_\theta) \boldsymbol{e}_\theta \quad \text{as} \quad r \to \infty, \tag{B13}$$

so

$$\boldsymbol{\nabla} \cdot \boldsymbol{v}_1 \to \left(2Z^E - (\eta/\ell^2) \frac{3}{\mathcal{E}} C^E \right) r^{-2} (\boldsymbol{E} \cdot \boldsymbol{e}_r) \quad \text{as} \quad r \to \infty \tag{B14}$$

and, hence,

$$\begin{aligned} \boldsymbol{f}_0' &= \frac{\mathcal{E}}{3} \int_{r \to \infty} \left[\left(\frac{\partial v_{0,i}}{\partial x_j} + \frac{\partial v_{0,j}}{\partial x_i} \right) + \frac{\partial v_{1,k}}{\partial x_k} \delta_{ij} \right] e_{r,j} \mathrm{d}A \\ &= \mathcal{E}(16/9) \pi Z^E \boldsymbol{E} + \mathcal{E}(8/9) \pi Z^E \boldsymbol{E} - (4/3) \pi (\eta/\ell^2) C^E \boldsymbol{E} \\ &= (8/3) \pi Z^E \mathcal{E} \boldsymbol{E} - (4/3) \pi (\eta/\ell^2) C^E \boldsymbol{E}. \end{aligned} \tag{B15}$$

Finally, adding the volume integral $[-(8/3)\pi(\eta/\ell^2) C^E \boldsymbol{E}]$ gives the net mechanical-contact force acting on the inclusion,

$$\boldsymbol{f}^{m,E} = (8/3) \pi Z^E \mathcal{E} \boldsymbol{E} - 4\pi (\eta/\ell^2) C^E \boldsymbol{E}. \tag{B16}$$

[1] A. M. Lowman, T. D. Dziubla, P. Bures, and N. A. Peppas, *Advances in Chemical Engineering*, 1st ed. (Elsevier, San Diego, 2004), Vol. 29, pp. 75–130.

[2] *Reflexive Polymers and Hydrogels*, edited by N. Yui, R. J. Mrsny, and K. Park (CRC Press, Boca Raton, FL, 2004).

[3] M. J. Bassetti, A. N. Chatterjee, N. R. Aluru, and D. J. Beebe, J. Microelectromech. Syst. **14**, 1198 (2005).

[4] M. A. Matos, L. R. White, and R. D. Tilton, J. Colloid Interface Sci. **300**, 429 (2006).

[5] R. J. Hill, J. Fluid Mech. **551**, 405 (2006).

[6] F. C. MacKintosh and C. F. Schmidt, Curr. Opin. Colloid Interface Sci. **4**, 300 (1999).

[7] E. M. Furst, Curr. Opin. Colloid Interface Sci. **10**, 79 (2005).

[8] M. R. Solomon and Q. Lu, Curr. Opin. Colloid Interface Sci. **6**, 430 (2001).

[9] N. Willenbacher and C. Oelschlaeger, Curr. Opin. Colloid Interface Sci. **12**, 43 (2007).

[10] W. B. Russel, D. A. Saville, and W. R. Schowalter, *Colloidal Dispersions* (Cambridge University Press, Cambridge, 1989).

[11] J. L. Anderson, Annu. Rev. Fluid Mech. **21**, 61 (1989).

[12] Here, the elastic restoring force is the value when a rigid sphere with radius a is embedded in an elastic continuum with Young's modulus $\mathcal{E}$ and Poisson's ratio $\nu = 0.5$.

[13] H. C. Brinkman, Appl. Sci. Res., Sect. A **1**, 27 (1949).

[14] F. Booth, Proc. R. Soc. London, Ser. A **203**, 514 (1950).
[15] R. J. Hill, J. Chem. Phys. **124**, 014901 (2006).
[16] R. W. O'Brien and L. R. White, J. Chem. Soc., Faraday Trans. 2 **74**, 1607 (1978).
[17] R. J. Hill, D. A. Saville, and W. B. Russel, J. Colloid Interface Sci. **258**, 56 (2003).
[18] R. J. Hill, Phys. Fluids **18**, 043103 (2006).
[19] L. D. Landau and E. M. Lifshitz, *Theory of Elasticity*, 3rd ed. (Pergamon, New York, 1986).
[20] M. Ostoja-Starzewski and C. Wang, Acta Mech. **80**, 61 (1989).
[21] X. Du and M. Ostoja-Starzewski, Proc. R. Soc. London, Ser. A **462**, 2949 (2006).
[22] M. Ostoja-Starzewski, *Microstructural Randomness and Scaling in Mechanics of Materials* (Chapman and Hall/CRC/Taylor and Francis, New York, 2007).
[23] K. Urayama, T. Takigawa, and T. Masuda, Macromolecules **26**, 3092 (1993).
[24] T. Takigawa, Y. Morino, K. Urayama, and T. Masuda, Polym. Gels Networks **4**, 1 (1996).
[25] B. Schnurr, F. Gittes, F. C. MacKintosh, and C. F. Schmidt, Macromolecules **30**, 7781 (1997).
[26] Assuming a constant *shear modulus* $\mathcal{E}/[2(1+\nu)]$ [19].
[27] T. Mura, I. Jasiuk, and B. Tsuchida, Int. J. Solids Struct. **21**, 1165 (1985).
[28] With a slipping boundary condition (i.e., zero radial displacement and zero tangential stress at $r=a$), the force is $-12\pi\mathcal{E}a\mathbf{Z}(1-\nu)/[(7-8\nu)(1+\nu)]$.
[29] A finite-difference scheme based on the methodology of Hill, Saville, and Russel [17] is adopted. This features an adaptive, nonuniform grid to handle the disparate length scales.
[30] The electrophoretic mobilities reported here were calculated using software (called MPEK, available from the corresponding author) based on the methodology of Hill, Saville, and Russel [17] for the electrophoretic mobility and other single-particle properties of spherical polymer-coated colloids. Here, the influence of a polymer coating is removed by specifying an infinite (large) Darcy permeability for the coating. The mobilities in Figs. 5 and 6 are in excellent agreement with the O'Brien and White calculations [16]; small differences can be attributed to the opposite sign of the ζ potential.
[31] T. M. Squires and J. F. Brady, Phys. Fluids **17**, 073101 (2005).
[32] Squires and Brady [31] present a compelling case to associate Sutherland with this famous relationship.
[33] P.-G. de Gennes, *Scaling Concepts in Polymer Physics* (Cornell University Press, New York, 1979).